Journal of Power Sources 216 (2012) 482–488

Contents lists available at SciVerse ScienceDirect

Journal of Power Sources

journal homepage: www.elsevier.com/locate/jpowsour

Effect of doping $LiMn_2O_4$ spinel with a tetravalent species such as Si(IV) versus with a trivalent species such as Ga(III). Electrochemical, magnetic and ESR study

A. Iturrondobeitia [a], A. Goñi [a], V. Palomares [a], I. Gil de Muro [a], L. Lezama [a], T. Rojo [a,b,*]

[a] Departamento de Química Inorgánica, Universidad del País Vasco UPV/EHU, P.O. Box 644, 48080 Bilbao, Spain
[b] CIC ENERGIGUNE, Parque Tecnológico de Álava, Albert Einstein 46, ED.E7, Of. 206, 01510 Miñano, Spain

HIGHLIGHTS

- We synthesize three spinel compounds for lithium ion batteries.
- Si insertion leads to more expanded and regular MnO_6 octahedra.
- Magnetic measurements corroborate the insertion of the dopants.
- $LiMn_{1.95}Si_{0.05}O_4$ gives the best electrochemical performance.

ARTICLE INFO

Article history:
Received 26 March 2012
Received in revised form
29 May 2012
Accepted 5 June 2012
Available online 19 June 2012

Keywords:
Doped spinel
Cathode
Structural stability
Lithium-ion batteries
Magnetic disorder
Improved specific capacity

ABSTRACT

Three cathode compounds for lithium ion batteries, $LiMn_2O_4$, $LiMn_{1.95}Si_{0.05}O_4$ and $LiMn_{1.9}Ga_{0.1}O_4$ have been synthesized by the freeze-drying method. All samples present partially sintered particles of 80 nm average size, corresponding to single crystalline phases with cubic spinel structure. The substitution of a little portion of Mn(IV) by Si(IV) in the crystal framework leads to more expanded and regular MnO_6 octahedra, whereas the replacement of some Mn(III) by Ga(III) induces the opposing effect. The ESR measurements support the effectiveness of doping as an evolution of the width of the resonance signal with the composition is observed. A complete magnetic study has been carried out, including ac and dc magnetic susceptibility measurements at different fields, FC and ZFC, and magnetization versus field. Due to the in-built magnetic frustration in spinel structure and the competition between different exchange pathways, the insertion of small quantities of dopants causes significant differences in the magnetic behaviour. The electrochemical study has revealed very good values of specific capacity for $LiMn_{1.95}Si_{0.05}O_4$ reaching 146 mA h g^{-1} and 139 mA h g^{-1} at C/10 and 1C rates, respectively. A capacity retention up to 75% has been observed for the three samples after 300th cycles.

1. Introduction

The actual research on battery materials is moving towards developing electrodes on the basis of abundance and availability of the relevant chemicals. In this sense, materials centred on sustainable 3d metal redox elements such as $LiMn_2O_4$ are receiving increased attention [1]. Lithium manganese oxide spinel is specially interesting for use in hybrid electric vehicles (HEV) and electric vehicles (EV) due to its low cost and high safety [2,3]. However, for the practical application, this compound must overcome the capacity loss originated by the volume change and phase separation associated to the Jahn–Teller distortion of the Mn(III) species [4,5]. This issue is aggravated by the progressive dissolution of manganese in the electrolyte as a result of surface disproportionation reaction of Mn(III) into Mn(II) and Mn(IV) [6]. The most extended solution for this problem is doping the manganese sites with trivalent or divalent cations because the resultant Mn(III) content is reduced [7,8]. In this sense, little amounts of several elements [9–13] have been found to be effective for doping, leading to electrodic materials with lower capacity decay. However, the restriction of the amount of the oxidizable Mn(III) species limits the maximum value of the specific capacity which can be reached in the 3.5–4.2 V range. Thus, the substitution of a little amount of Mn(IV) by a tetravalent dopant as Si(IV) can be another solution, in order to stabilize the spinel framework without any decrease of the amount of the electroactive Mn(III) cation.

* Corresponding author. Departamento de Química Inorgánica, Universidad del País Vasco UPV/EHU, P.O. Box 644, 48080 Bilbao, Spain. Tel.: +34 946012458; fax: +34 946013500.
E-mail address: teo.rojo@ehu.es (T. Rojo).

0378-7753/$ – see front matter © 2012 Elsevier B.V. All rights reserved.
http://dx.doi.org/10.1016/j.jpowsour.2012.06.031

Most of the lithium intercalation compounds suitable for their use as positive electrodes exhibit enhanced electrochemical properties when they have been prepared in the form of nanoparticles [14,15]. In this sense, we have selected a freeze-drying synthesis procedure to obtain nanostructured samples with homogeneous distribution of the dopants. This procedure has been already proved to be useful to generate nanosized cathodic materials with remarkable electrochemical performance [16,17].

In this paper, we report an investigation on the effect of doping $LiMn_2O_4$ with a tetravalent species such as Si(IV) and a trivalent cation such as Ga(III) for comparison, trying to find a cathode material with high discharge capacity as well as good capacity retention. The magnetic and electrochemical studies allow establishing the correlation between the composition, morphology, physico-chemical properties and the electrochemical performance.

2. Experimental

2.1. Materials and reagents

The following materials and reagents were used: citric acid monohydrate (%99.5, Sigma–Aldrich), manganese (III) acetate dihydrate (%97, Sigma–Aldrich), lithium hydroxide monohydrate (%99, Fluka), silicon acetate (%99, Alfa Aesar) and gallium nitrate (% 99.99, Sigma–Aldrich).

2.2. Synthesis of undoped and doped spinels

$LiMn_2O_4$, $LiMn_{1.95}Si_{0.05}O_4$ and $LiMn_{1.9}Ga_{0.1}O_4$ were synthesized by freeze-drying method. Citric acid monohydrate ($C_6H_8O_7\cdot H_2O$), manganese (III) acetate dihydrate ($Mn(C_2H_3O_2)_3\cdot 2H_2O$) and lithium hydroxide monohydrate ($LiOH\cdot H_2O$) were dissolved in 25 ml of water with a molar ratio of 3:1:1. The dissolution obtained was then frozen in a round-bottom flask that contained liquid nitrogen. In the case of the gallium doped phase, $LiMn_{1.9}Ga_{0.1}O_4$, citric acid monohydrate ($C_6H_8O_7\cdot H_2O$), manganese (II) nitrate ($Mn(NO_3)_2$), gallium nitrate ($Ga(NO_3)_3$) and lithium hydroxide monohydrate ($LiOH\cdot H_2O$) were dissolved in 25 ml of water with a molar ratio of 3:1.9:0.1.1. The silicon doped phase, $LiMn_{1.95}Si_{0.05}O_4$, was obtained by mixing citric acid monohydrate ($C_6H_8O_7\cdot H_2O$), manganese (III) acetate dihydrate ($Mn(C_2H_3O_2)_3\cdot 2H_2O$), silicon acetate ($Si(CH_3COO)_4$) and lithium hydroxide monohydrate ($LiOH\cdot H_2O$) with a molar ratio of 3:1.95:0.05:1. After solutions were frozen, the round-bottom flasks were connected to the freeze-dryer to produce the sublimation of the solvent, at a pressure of $3\cdot 10^{-1}$ mbar and a temperature of −80 °C. Then, the obtained precursors were subjected to a heat treatment at 700 °C. Subsequently, phases were ball-milled.

2.3. Characterization and electrochemical measurements

Structural characterization of the composites was performed by powder X-ray diffraction using a Bruker D8 Advance Vario diffractometer working with CuK_α radiation. Obtained diffractograms were fitted using the FULLPROF program. Morphology of the materials was observed by Transmission Electron Microscopy (TEM) in a Philips CM200 microscope equipped with an EDAX energy dispersive X-ray analysis (EDX). A Bruker ELEXSYS 500 spectrometer equipped with a super-high-Q resonator ER-4123-SHQ, operating at X band, was used to record the ESR polycrystalline spectra. Magnetic susceptibility measurements (dc) were carried out in a Quantum Design SQUID magnetometer between 5 K and 300 K. For the ac magnetic susceptibility, we used a standard Quantum Design PPMS system with an alternate excitation field of 1 Oe and frequencies between 10^2 and 10^4 Hz.

Electrochemical tests were conducted using Swagelok-type cells assembled in an environmentally controlled dry box. The negative electrode was a disk of lithium metal foil. A porous glass microfiber sheet soaked in a solution of 1 M $LiPF_6$ in ethylene carbonate–dimethyl carbonate (1:1 in volume) was placed between the two electrodes. The composite positive electrode contained 20% of S-black, 5% of poly(vinylidenefluoride) binder, and 75 wt % of active material. The galvanostatic tests were carried out by using a Bio-Logic VMP3 battery tester at different current rates from C/10 to 10C in the range from 3.2 to 4.5 V versus Li/Li^+.

3. Results and discussion

Three $LiMn_2O_4$, $LiMn_{1.95}Si_{0.05}O_4$ and $LiMn_{1.9}Ga_{0.1}O_4$ samples were characterized by X-ray diffraction at room temperature. The diffraction peaks observed in the XRD pattern for $LiMn_2O_4$ (Fig. 1) correlate to pure phase cubic spinel with an experimental cell parameter of 8.2353(7) Å (Powder Diffraction File 89-0118 PDF card). It cannot be noticed any strange reflection, thus no impurities were detected. XRD pattern of 2.5% silicon doped $LiMn_{1.95}Si_{0.05}O_4$ sample (Fig. 1b) also corresponded to a single crystalline phase with cubic spinel structure. It was indexed with the same cubic Fd-3m space group of $LiMn_2O_4$. As a consequence of Si(IV) doping, the cell parameter is slightly increased to 8.2369(8) Å. The XRD pattern of the gallium doped $LiMn_{1.9}Ga_{0.1}O_4$ phase (Fig. 1c) is also similar to that observed for pure spinel. The value of the cell parameter is reduced down to 8.2165(7) Å by Ga(III) doping.

Small differences can be observed by comparing the diffraction patterns of the three samples. In both doped compounds, some XRD peaks show a slightly lower intensity and little widening, indicative of a certain crystallographic disorder induced by the insertion of dopants in the framework. According to Capsoni et al., the dopant ions could be located on both spinel metal sites, octahedral *16d* and tetrahedral *8a*. However, if dopant species locates at tetrahedral site, the intensity of *220* reflection at $2\theta \approx 30°$ must increase its intensity, even at very low substitution percentages [18].

This fact is not evidenced for any of the samples so it could be said that the tetrahedral sites (8a) are only occupied by lithium atoms which give undetectable (220) signal due to their very low X-ray scattering ability [6]. Therefore, Si(IV) and Ga(III) are placed in the octahedral (16d) manganese sites.

Rietveld analysis of the three diffraction patterns was carried out. The refined cell parameters, bond lengths and angles, and the obtained reliability factors are exposed in Table 1. Occupation factors for manganese and dopants located in the same crystal site were fixed according to compositional formula. It is interesting to

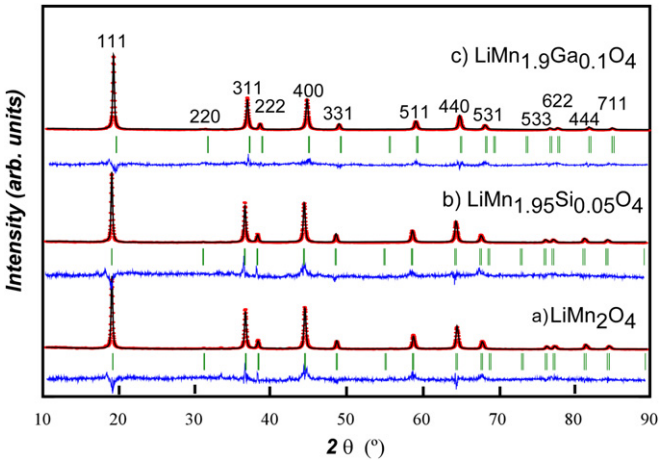

Fig. 1. X-ray pattern of a) $LiMn_2O_4$, b) $LiMn_{1.95}Si_{0.05}O_4$ and c) $LiMn_{1.9}Ga_{0.1}O_4$ samples.

Table 1
Cell parameters, cell volume, bond lengths, angles and reliability factors obtained for $LiMn_2O_4$, silicon doped sample $LiMn_{1.95}Si_{0.05}O_4$ and gallium doped sample $LiMn_{1.9}Ga_{0.1}O_4$.

Sample		$LiMn_2O_4$	$LiMn_{1.95}Si_{0.05}O_4$	$LiMn_{1.9}Ga_{0.1}O_4$
Cell parameter (Å)	$a = b = c$	8.2353 (7)	8.2369 (8)	8.2165 (7)
Cell volume (Å^3)		558.51 (1)	558.84 (1)	554.71 (1)
Bond lengths (Å)	Mn–O	1.998 (4)	2.009 (5)	1.991 (4)
	Li–O	1.891 (4)	1.873 (5)	1.893 (4)
Angles (°)	O–Mn–O	86.4	87.0	86.2
	O–Li–O	109.5	109.5	109.5
Reliability factors	χ^2	3.30	4.80	5.67
	R_p	10.5	11.5	10.2
	R_{wp}	14.8	16.8	16.2

note that even if the ionic radium of Si(IV) [r = 0.40 Å] is smaller than that of the Ga(III) [r = 0.62 Å] in octahedral site, the cell volume is increased when Si(IV) partially replaces Mn(IV) [r = 0.53 Å], and it is reduced when Ga(III) substitutes Mn(III) [r = 0.58 Å]. In this sense, the Mn–O bond lengths and so, the size of the MnO_6 octahedra are larger in $LiMn_{1.95}Si_{0.05}O_4$ than in $LiMn_2O_4$ and $LiMn_{1.9}Ga_{0.1}O_4$. Moreover, in silicon doped phase the O–Mn–O angles present values more close to 90°, corresponding to a slightly more regular octahedron. This way, the insertion of Si(IV) in spinel provides more expanded and regular MnO_6 octahedra, suitable for a better accomodation of the Mn(III)–Mn(IV) interconversion during the lithium deintercalation and intercalation [19].

Morphologic study of $LiMn_2O_4$, $LiMn_{1.95}Si_{0.05}O_4$ and $Li_1Mn_{1.9}Ga_{0.1}O_4$ was carried out by TEM. The selected micrographs for $LiMn_{1.95}Si_{0.05}O_4$ phase (Fig. 2) show the presence of homogeneous particles of 80 nm average size. The crystals, which do not present a regular shape, are partially sintered. For the other two samples the morphology is very similar because of the same synthetic conditions. The freeze-drying method, employing medium annealing temperatures, 700 °C, has led to medium grain sizes in three samples. Moreover, at 700 °C the sintering process has started, improving the connection between the particles.

The ESR spectra of $LiMn_2O_4$, $LiMn_{1.95}Si_{0.05}O_4$ and $LiMn_{1.9}Ga_{0.1}O_4$ were recorded at X band at room temperature (Fig. 3). Similar pattern was observed in the three cases: a very broad quasi-isotropic signal centred at a Lande' factor **g** close to 2. This signal is characteristic of exchange coupled Mn(IV)–Mn(III) ions. The **g** value calculated for the three spectra does not exhibit any variation in function of the chemical composition. However, the linewidth of the signal shows a clear dependence with the Mn(III)/Mn(IV) proportion. The peak-to-peak linewidth ΔHpp value is wider than 2500 Oe for all cases (see inset in Fig. 3), and experiments a clear enlargement with the increase of the Mn(III)/Mn(IV) rate. In this sense, the ΔHpp measured for $LiMn_{1.9}Ga_{0.1}O_4$, with the lowest Mn(III) quantity, is the narrowest one, 2690 Oe. By the contrary, for $LiMn_{1.95}Si_{0.05}O_4$, with Mn(III)/Mn(IV) rate equal to 1.05, the linewidth widens up to 3150 Oe.

The short spin-lattice relaxation time and large zero-field splitting of Mn(III) hinder to observe any paramagnetic resonance absorption at X-band corresponding to this ion. However, the magnetic coupling between the Mn(III) and Mn(IV) ions induces a significant broadening of the absorption band of Mn(IV), affected by the short spin-lattice relaxation times of Mn(III). Thus, the broadening effect is more perceptible as the relative content of Mn(III) is greater. Therefore, this technique supports the existence of an effective doping in spinel.

Magnetic susceptibility measurements for both doped phases were carried out in the 5–300 K temperature range, at two different magnetic fields: 100 Oe and 1 kOe. Fig. 4 exhibits the thermal evolution of molar susceptibility for field cooled (FC) and zero field cooled (ZFC) $LiMn_{1.95}Si_{0.05}O_4$. In ZFC curves at both mentioned different fields, a maximum in χ_m is observed at 23 K, which is indicative of predominant antiferromagnetic interactions. However, the FC and ZFC curves diverge from 45 K, showing the appearing of a phenomenon of weak ferromagnetism below that temperature. The magnitude of the divergence is dependent on the applied field. At stronger field the ferromagnetic component diminishes, so this remnant moment comes into being as a result of the antiferromagnetic ordering. The value of the calculated magnetic moment at 300 K, $\mu_{eff} = \sqrt{8\chi_m T} = 2.45\ \mu_B$ per mol of Mn, is significantly lower than that expected for a Mn(III)–Mn(IV) system, in good agreement with the existence of short-range antiferromagnetic interactions also from room temperature. Moreover, the inverse of the susceptibility (inset of Fig. 4) does not fit a Curie–Weiss behaviour, confirming the existence of strong antiferromagnetic interactions in all temperature range.

Fig. 5 shows the thermal evolution of χ_m for $LiMn_{1.9}Ga_{0.1}O_4$, at 100 Oe and 1 kOe. FC and ZFC measurements were also performed. In this case, the maximum in the susceptibility is observed at 16 K. Furthermore, the hysteresis between the ZFC and FC curves starts down to 45 K, but becomes much more clear at a temperature close to the maximum in χ_m. Thus, this phase also presents a main antiferromagnetic behaviour with the existence of a weak

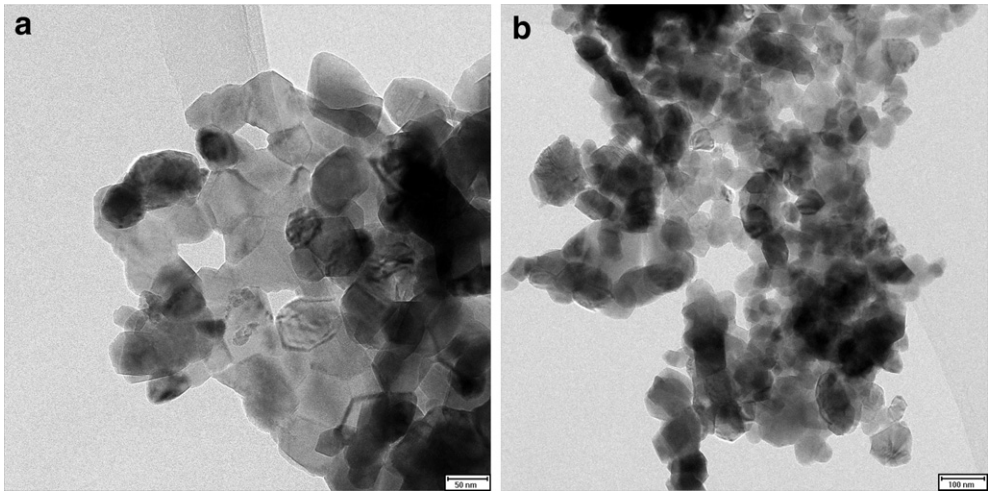

Fig. 2. TEM micrographs of the silicon doped sample $LiMn_{1.95}Si_{0.05}O_4$.

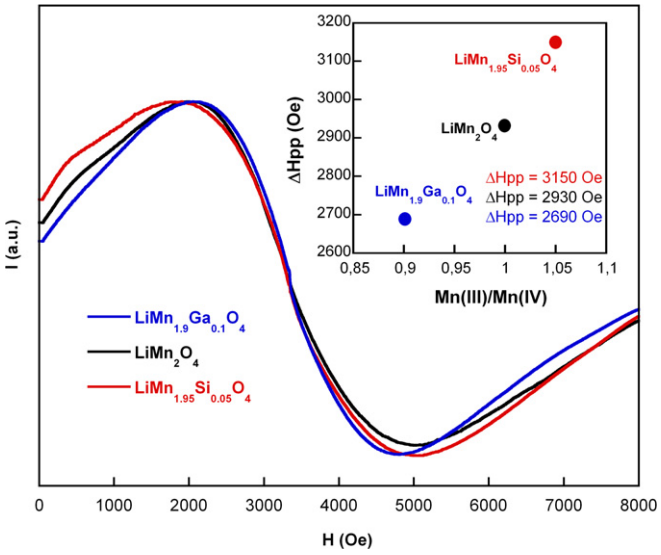

Fig. 3. ESR spectra at X band at room temperature. Inset: peak-to-peak linewidth (ΔHpp) in function of the Mn(III)/Mn(IV) rate.

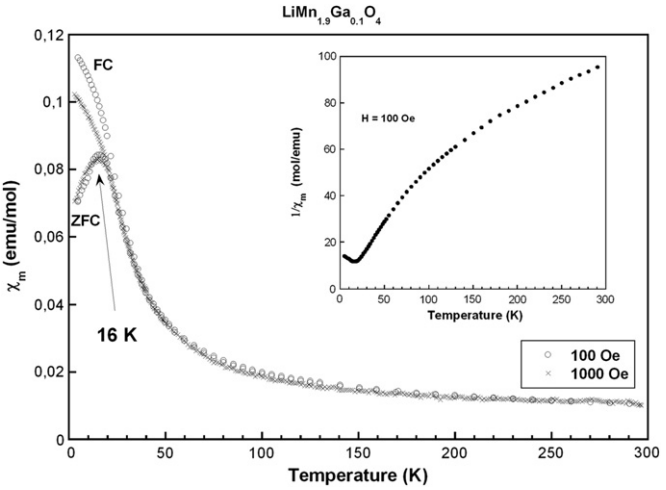

Fig. 5. The thermal evolution of χ_m for $LiMn_{1.9}Ga_{0.1}O_4$, at FC and ZFC. Inset: inverse of the susceptibility.

ferromagnetic component at low temperature. The inset of the graphic shows an image of the thermal evolution of $1/\chi_m$. No paramagnetic behaviour is observed in all the studied temperature range. The low value of the calculated magnetic moment at 300 K, $\mu_{eff} = 2.62\ \mu_B$ per mol of Mn, accords with the presence of magnetic interactions from RT.

In order to determine the thermal evolution of the weak ferromagnetic component at low temperatures, field cooled magnetization versus temperature data were also collected. The plots obtained for both doped samples are given in Fig. 6. In the case of $LiMn_{1.95}Si_{0.05}O_4$, M progressively decreases by heating the sample from 5 K up to 45 K. For $LiMn_{1.9}Ga_{0.1}O_4$, a deep decrease of magnetization is observed from 5 K up to 20 K. At this point, the thermal evolution of M exhibits a clear change to a softer slope. Saturation is not observed for both compounds. The magnetization hysteresis loops measured at 3 K for silicon and gallium doped spinels are represented in the inset of Fig. 6. The values of coercive field and magnetization at zero field are 2500 Oe and 0.016 μ_B mol^{-1} for $LiMn_{1.95}Si_{0.05}O_4$, and 1700 Oe and 0.025 μ_B mol^{-1} for $LiMn_{1.9}Ga_{0.1}O_4$, respectively. The gallium doped phase presents a smaller value of coercive field, which is indicative of a lower resistance of the magnetic moments to the applied field at that temperature.

The ac susceptibility data were collected by different applied fields, and at different frequencies in the range from 100 to 10,000 Hz. A selection of curves is represented in Fig. 7. As can be observed, both doped compounds show broad maxima in the thermal evolution of χ'_m and χ''_m, but the curves of the silicon doped compound exhibit wider peaks as a result of a more disordered magnetic transition. The ferromagnetic component that appears in the magnetic arrangement is revealed by the peak in the imaginary susceptibility χ''_m that accompanies the peak in χ'_m. The maxima of ac susceptibility are centred at around 28 K for $LiMn_{1.95}Si_{0.05}O_4$ and 21 K for $LiMn_{1.9}Ga_{0.1}O_4$. Those temperatures do not experiment any evolution by changing frequencies or magnetic fields. This fact allows discarding a spin-glass-like behaviour for the samples.

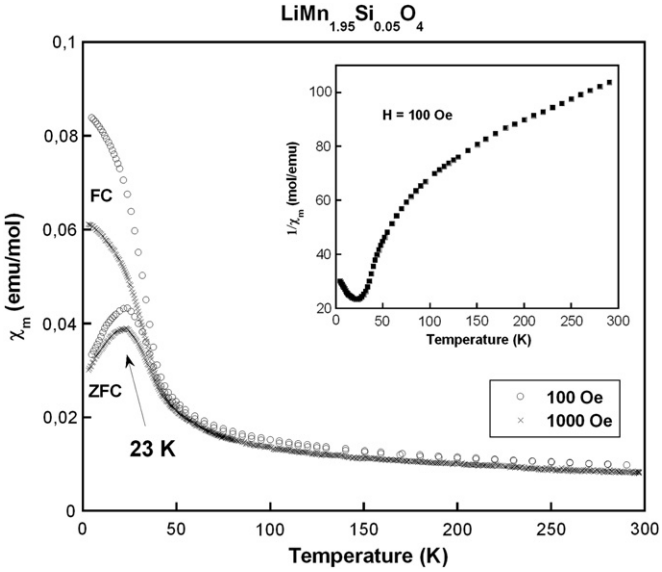

Fig. 4. Thermal evolution of molar susceptibility for field cooled (FC) and zero field cooled (ZFC) $LiMn_{1.95}Si_{0.05}O_4$. Inset: inverse of the susceptibility.

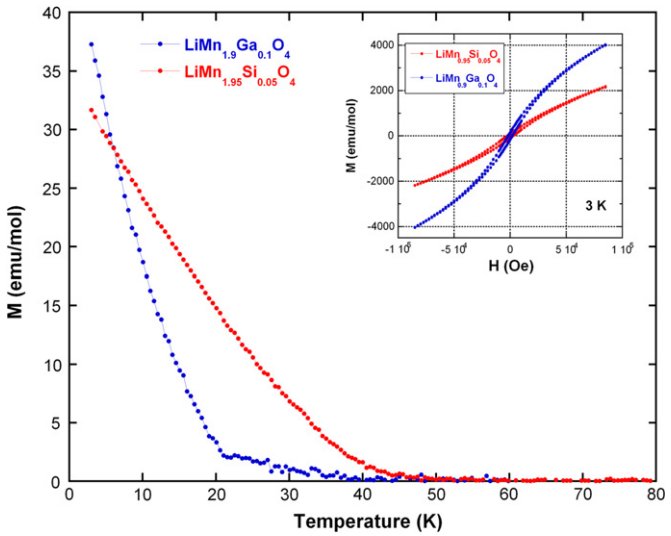

Fig. 6. Field cooled magnetization versus temperature data. Inset: magnetization hysteresis loops measured at 3 K.

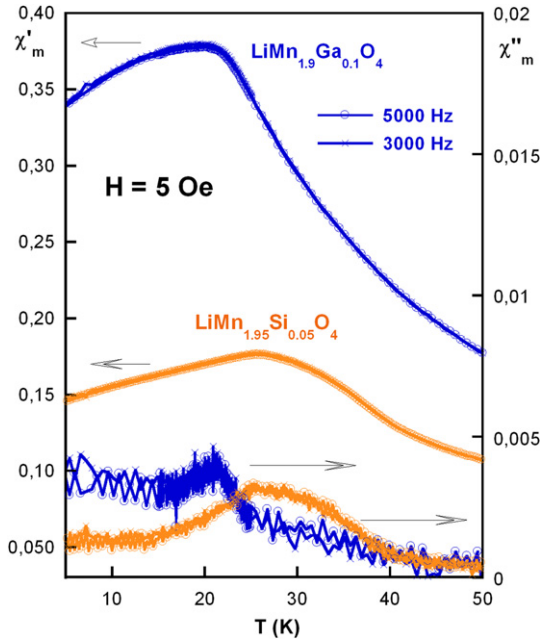

Fig. 7. Selected curves of ac susceptibility collected at different frequencies.

The Mn sublattice in the $LiMn_2O_4$ parent spinel satisfies the condition of a magnetic frustrated system [20]. The dominant antiferromagnetic exchange interactions are geometrically frustrated in the cubic structure because the four magnetic moments of the Mn ions located at the vertexes of a tetrahedron cannot align themselves in such a way as to be simultaneously antiparallel to each other. In addition, superexchange 90° $Mn^{III/IV}$–O–$Mn^{III/IV}$ interactions are also conceivable between the nearest Mn neighbours. According to Goodenough's rules [21], only 90° Mn^{IV}–O–Mn^{IV} coupling will be ferromagnetic, while all other possibilities will be antiferromagnetic. Thus, a spin-glass-like behaviour has been reported for some $LiMn_2O_4$ spinel samples, as a result of the magnetic disorder generated by the frustration and the existence of different contending magnetic interactions [22,23]. However, other possibilities such as a canted antiferromagnetic ordering of spins, and the coexistence of a long-range ordered state with a significant fraction of spins remaining disordered at low temperatures have been also published [24].

In the case of $LiMn_{1.9}Ga_{0.1}O_4$ and $LiMn_{1.95}Si_{0.05}O_4$ doped spinel samples, the spin-glass like behaviour has been discarded by the analysis of the ac susceptibility measurements. The nature of the weak ferromagnetic component at low temperature, as well as the extent of the temperature range for the magnetic transition (broad χ''_m maxima), indicate the existence of a complex magnetic behaviour with the presence of partially ordered magnetic clusters of different sizes, as a result of frustration and short-range competing magnetic interactions. The substitution of 0.1 mol of Mn(III) by Ga(III), a non-magnetic metal, in $LiMn_{1.9}Ga_{0.1}O_4$ weakens the main magnetic interactions shifting the temperature of maximum in susceptibility towards a lower value. However, the substitution of Mn(IV) by a smaller amount of also non-magnetic Si(IV) in $LiMn_{1.95}Si_{0.05}O_4$ encourages the competition between the different magnetic exchange pathways, enlarging the range of temperatures for the magnetic transition. The different short-range spin correlations inside several clusters lead to a more disordered magnetic system.

The charge–discharge characteristics of $LiMn_2O_4$, $LiMn_{1.9}Ga_{0.1}O_4$ and $LiMn_{1.95}Si_{0.05}O_4$ were galvanostatically studied at a current rate of C/10 and 1C. Fig. 8 exhibits the first cycle of the three samples at C/10. As can be observed, the initial discharge capacity of the undoped spinel was 134 mA h g^{-1}. This value increased to 146 mA h g^{-1} for $LiMn_{1.95}Si_{0.05}O_4$, but decreased to 99 mA h g^{-1} for $LiMn_{1.9}Ga_{0.1}O_4$. At 1C, the capacity values were 131, 139 and 95 mA h g^{-1} for undoped sample, silicon, and gallium doped compounds, respectively. In all cases, accelerating by tenfold the discharge rate, the capacity loss is lower than 5%.

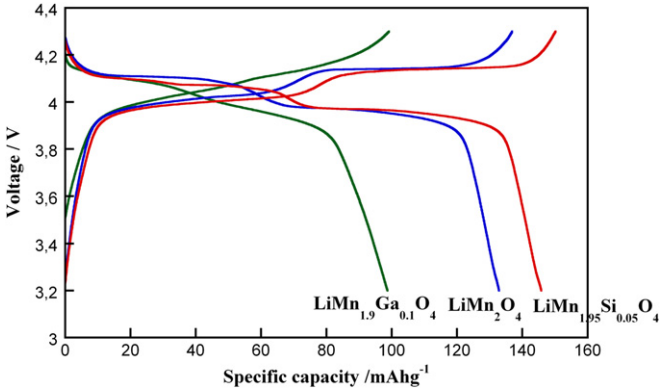

Fig. 8. Initial charge–discharge curves of $LiMn_2O_4$, $LiMn_{1.95}Si_{0.05}O_4$ and $LiMn_{1.9}Ga_{0.1}O_4$ samples.

In manganese pure spinel and silicon doped sample, the two voltage plateaus in 4 V region are obvious. However, in $LiMn_{1.9}Ga_{0.1}O_4$ the existence of both plateaus is not so evident. This sample exhibits more diffuse pseudo-plateaus with a continuous evolution of the voltage by charging or discharging. Moreover, this phase clearly offers lower specific capacity than that given by the other two compounds. This fact could be ascribed to the substitution of a portion of the redox active Mn(III) species by the inactive Ga(III) ion, reducing the possibility of a total deinsertion of lithium. On the other hand, $LiMn_{1.95}Si_{0.05}O_4$ gives the best specific capacity, reaching a value very close to the nominal one. This way the reversible extraction of all lithium is favoured by the total oxidation of Mn(III) to Mn(IV). Moreover, the galvanostatic cycle for this sample shows the lowest polarization, as the difference between the charge and discharge voltages is smaller than that observed for the other two phases. This feature can be due to the structural stabilization that Si(IV) doping provides, supporting the motion of the lithium ions by the Mn(III)–Mn(IV) redox exchange.

Cyclability studies were carried out by testing $LiMn_2O_4$, $LiMn_{1.95}Si_{0.05}O_4$ and $LiMn_{1.9}Ga_{0.1}O_4$ samples for more than 300

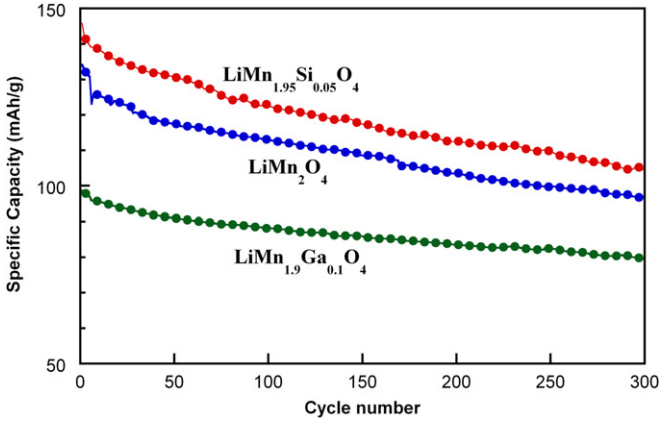

Fig. 9. Cycling performance of $LiMn_2O_4$, $LiMn_{1.95}Si_{0.05}O_4$ and $LiMn_{1.9}Ga_{0.1}O_4$ samples.

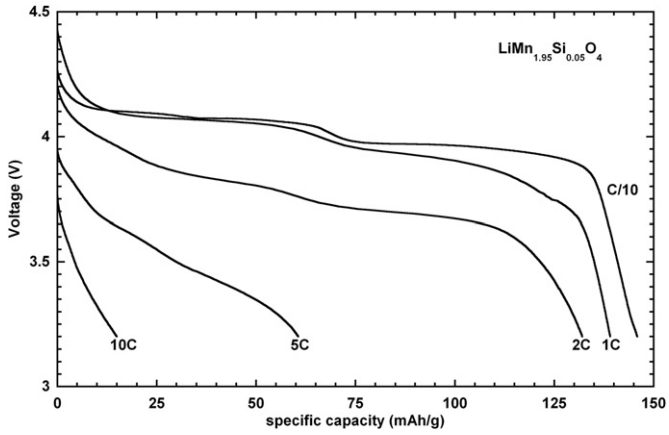

Fig. 10. Discharge curves of the $LiMn_{1.95}Si_{0.05}O_4$ sample at different current rates.

cycles at 1C (Fig. 9). At the 300th cycle, the capacity retention for all compounds was up 75%. The gallium doped sample shows a slightly better cycling performance, retaining the 85% of the initial capacity value after 300 cycles, as a consequence of its lesser content of Mn(III). By the contrary, although the Si(IV) insertion improves the overall specific capacity by allowing the deinsertion of most of the Li^+, the cycling performance of $LiMn_{1.95}Si_{0.05}O_4$ remains the same as that observed for the pure $LiMn_2O_4$ obtained by the same synthetic method.

To further investigate the electrochemical response of these materials, a charge-discharge study at different rates ranging from C/10 (14.8 mA g^{-1}) to 10C (1480 mA g^{-1}) was carried out. The electrodic mixture composition was not modified. Fig. 10 gives the discharge curves of the $LiMn_{1.95}Si_{0.05}O_4$ sample. At low and medium rates the material displays the characteristic features of the lithium manganese spinel, with two obvious voltage plateaus. As the current rate increases, the pseudo-plateaus are distorted and moved down to lower voltage values as a result of the deviation from equilibrium operating conditions.

The comparison of the rate capability between the undoped and the silicon doped spinel has been evaluated (Fig. 11). Due to the limited diffusion rate of the lithium ions in the cells, both samples show decreased capacities at high rates. However, $LiMn_{1.95}Si_{0.05}O_4$ delivers 135 mA h g^{-1} at 2C whereas the undoped sample could deliver only 120 mA h g^{-1} at the same rate. Moreover, after an exigent demand cycling, the discharge capacity of the doped spinel is better recovered at 2C as the Si(IV) doping provides a structural stabilization.

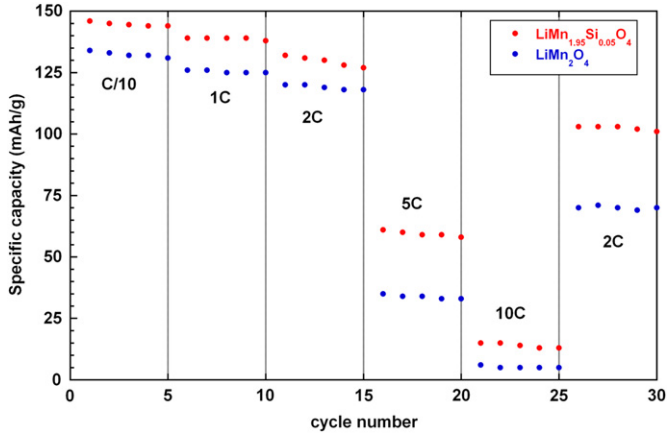

Fig. 11. Comparison of the rate capability between the undoped and the silicon doped spinel.

4. Conclusions

The freeze-drying method is a useful synthetic procedure to obtain pure $LiMn_2O_4$ spinel, and $LiMn_{1.95}Si_{0.05}O_4$ and $LiMn_{1.9}Ga_{0.1}O_4$ doped compounds. Homogeneous and semisintered samples with intermediate particle sizes have been obtained as a result of the employment of a short heat treatment at 700 °C. The presence of bulk particles that consist of aggregated nanosized particles provides good capacity values at current rates up to 2C. The introduction of dopants, Si(IV) in substitution of Mn(IV) or Ga(III) replacing Mn(III), have been evidenced by the presence of modifications in the crystallographic parameters, and also by the observed evolution in the spectroscopic and magnetic properties. The cationic disorder induced by doping, together with the in-built magnetic frustration of the spinel structure originate a complex magnetic behaviour in which different short-range interactions are competing. Thus, although a spin-glass-like behaviour has not been observed for any of the studied phases, the nature of the weak ferromagnetic component at low temperatures indicate the existence of magnetic clusters of many types. The $LiMn_{1.95}Si_{0.05}O_4$ compound, as a result of its higher Mn(III)/Mn(IV) proportion, exhibits stronger antiferromagnetic interactions, and thus the ordering temperature range is displaced towards upper values. Moreover, this phase gives better specific capacity values than those provide by pure spinel, because the reversible extraction of all lithium by Mn(III) oxidation is favoured. The presence of Si(IV) in the structure induces more expanded and regular MnO_6 octahedra suitable for a more easy accomodation for the Mn(III)–Mn(IV) change. However, the cycling performance is just as observed for the undoped phase. Consequently, additional strategies, such as coating and so on, must be also considered to preserve the exceptional specific capacity of the silicon doped spinel.

Acknowledgements

This work was financially supported by the Ministerio de Ciencia e Innovación (MAT2010-19442), the Universidad del Pais Vasco/Euskal Herriko Unibertsitatea (GIU06-11) and the Gobierno Vasco/Eusko Jaurlaritza (ETORTEK CICENERGIGUNE10, SAIOTEK S-PE11UN064). A.I. thanks the Gobierno Vasco/Eusko Jaurlaritza for a grant.

References

[1] B. Dunn, H. Kamath, J.M. Tarascon, Science 334 (2011) 928.
[2] M. Armand, J.M. Tarascon, Nature 451 (2008) 652.
[3] J.M. Tarascon, Phys. Trans. R. Soc. A 368 (2010) 3227.
[4] Y. Shin, A. Manthiram, Chem. Mater. 15 (2003) 2954.
[5] Y. Shin, A. Manthiram, J. Electrochem. Soc. 151 (2004) A204.
[6] L. Xiong, Y. Xu, T. Tao, J.B. Goodenough, J. Power Sources 199 (2012) 214–219.
[7] W.H. Ryu, J.Y. Eom, R.Z. Yin, D.W. Han, W.K. Kim, H.S. Kwon, J. Mater. Chem. 21 (39) (2011) 15337.
[8] R. Thirunakaran, A. Sivashanmugan, S. Gopukumar, R. Rajalakshmi, J. Power Sources 187 (2009) 565.
[9] A. Yuan, L. Tian, W. Xu, Y. Wang, J. Power Sources 195 (2010) 5032.
[10] P. Singh, A. Sil, M. Nath, S. Ray, J. Electrochem. Soc. 157 (3) (2010) A259.
[11] R. Thirunakaran, K.T. Kim, Y.M. Kang, C.Y. Seo, J. Young-Lee, J. Power Sources 137 (2004) 100.
[12] S. Patoux, L. Sannier, H. Lignier, Y. Reinyer, C. Bourbon, S. Jouanneau, F.L. Cras, S. Martinet, Electrochim. Acta 53 (2008) 4137.
[13] D.Q. Liu, Z.Z. He, X.Q. Liu, J. Alloys Compd. 440 (2007) 69.
[14] C. Liu, F. Li, L.P. Ma, H.M. Cheng, Adv. Mater. 22 (2010) E28.
[15] P. Bruce, B. Scrosati, J.M. Tarascon, Angew. Chem. Int. Ed. 47 (2008) 2930.
[16] V. Palomares, A. Goñi, I. Gil de Muro, I. de Meatza, M. Bengoechea, I. Cantero, T. Rojo, J. Electrochem. Soc. 156 (10) (2009) A817.
[17] V. Palomares, A. Goñi, I. Gil de Muro, I. de Meatza, M. Bengoechea, O. Miguel, T. Rojo, J. Power Sources 171 (2007) 879.

[18] D. Capsoni, M. Bini, G. Chiodelli, P. Mustarelli, V. Massarotti, C.B. Azzoni, M.C. Mozzati, L. Linati, J. Phys. Chem. B 106 (2002) 7432.
[19] D. Arumugam, G.P. Kalaignan, K. Vediappan, C.W. Lee, Electrochim. Acta 55 (2010) 8439–8444.
[20] J.E. Greendan, N.P. Raju, A.S. Wills, C. Morin, S.M. Shaw, Chem. Mater. 10 (1998) 3058.
[21] J.B. Goodenough, Magnetism and the Chemical Bond, Wiley, New York, 1963.
[22] Y.I. Jang, F.C. Chou, Y.M. Chiang, Appl. Phys. Lett. 74 (17) (1999) 2504.
[23] V. Kusigerski, D. Markovic, V. Spasojevic, N. Cvjeticanin, M. Mitric, D. Jugovic, D. Uskokovic, J. Magn. Mater. 320 (6) (2008) 943.
[24] A.S. Wills, N.P. Raju, J.E. Greendan, Chem. Mater. 11 (1999) 1510.